CHEMISTRY OF MATERIALS
Article

Chem. Mater. **2010,** *22,* 2555–2562 2555
DOI:10.1021/cm9035659

Photoelectrochemical Response of $TlVO_4$ and $InVO_4$:$TlVO_4$ Composite

Dennis P. Butcher, Jr. and Andrew A. Gewirth*

Department of Chemistry, University of Illinois at Urbana−Champaign, 600 S. Mathews Avenue, Urbana, Illinois 61801

Received November 24, 2009. Revised Manuscript Received March 4, 2010

This work presents photoelectrochemical characteristics of $TlVO_4$, a previously uncharacterized candidate for photocatalytic water splitting. Additionally, a composite of $InVO_4$ and $TlVO_4$ was synthesized by a facile solution method using orthorhombic $InVO_4$ as a seed for growth of crystallographically similar orthorhombic $TlVO_4$. Photoelectrochemical measurements indicate an increase in photocurrent and more negative flatband potentials for $TlVO_4$ and the $InVO_4$:$TlVO_4$ composite relative to $InVO_4$. Diffuse reflectance UV−visible measurements were used to determine bandgaps of 3.50 eV, 2.94 eV, and 2.98 eV for $InVO_4$, $TlVO_4$, and $InVO_4$:$TlVO_4$, respectively. Density functional theory (DFT) calculations were performed to elucidate the band structures and correlate well with experimental data. The results indicate higher photoelectrochemical activity for $TlVO_4$ and the $InVO_4$:$TlVO_4$ composite relative to $InVO_4$.

I. Introduction

There are considerable economic, environmental, and security benefits involved in transitioning to a hydrogen based economy.[1−8] The discovery of photoelectrochemical hydrogen evolution on TiO_2 by Fujishima and Honda in 1972[9] sparked intense research efforts into overall water splitting by semiconductor photocatalysis with the hope of attaining sustainable hydrogen production from solar energy. There remains considerable interest in overall water splitting today.[10] Particulate photocatalyst systems, which provide the advantages of simple cell construction and lower cost when compared to photoelectrochemical cells using massive or single crystal electrodes,[4] have received significant research attention since the early reports of overall water splitting in these systems in 1980.[11−13] Since those early reports, many photocatalyst systems have been catalogued,[14] though none approach commercially viable efficiency levels in visible light.

Semiconductor overall water splitting photocatalytic efficiency is limited by recombination of electron/hole pairs, fast back reactions of photocatalytic products, and insufficient visible light absorption.[7] The basic requirements of an effective total water splitting photocatalyst include strong visible absorption, stability toward photocorrosion, efficient charge transfer with limited recombination effects, low cost, and suitable band positions for water oxidation/reduction accompanied with low overpotentials.[15] The positions of the conduction and valence band edges of the semiconductor are particularly crucial to the photocatalytic activity. The conduction band must lie at potentials more negative than H^+/H_2 (0 V vs NHE at pH = 0) and the valence band must lie at potentials more positive than O_2/H_2O (1.23 V vs NHE at pH = 0).[16] Without these conditions being met, total water splitting cannot occur thermodynamically and must be driven by an external bias.

While a number of semiconductor materials are relatively efficient at hydrogen production, this efficiency often comes at a cost of diminished stability in the aggressive aqueous environment, particularly in the case of metal chalcogenides.[4,14,17] Metal oxides are generally stable enough to resist photocorrosion if the kinetics of water oxidation are faster than anodic decomposition, and have thus been the focus of many researchers as viable water splitting photocatalyst materials.[15] The primary

*To whom correspondence should be addressed. E-mail: agewirth@illinois.edu. Phone: +1-217-333-8329. Fax: +1-217-244-3186.

(1) Conte, M.; Iacobazzi, A.; Ronchetti, M.; Vellone, R. *J. Power Sources* **2001**, *100*, 171.
(2) Lewis, N. S.; Nocera, D. G. *Proc. Natl. Acad. Sci. U.S.A.* **2006**, *103*, 15729.
(3) Serrano, E.; Rus, G.; García-Martínez, J. *Renewable Sustainable Energy Rev.* **2009**, *13*, 2373.
(4) Yerga, R. M. N.; Galván, M. C. Á.; del Valle, F.; Villoria de la Mano, J. A.; Fierro, J. L. G. *ChemSusChem* **2009**, *2*, 471.
(5) Cortright, R. D.; Davda, R. R.; Dumesic, J. A. *Nature* **2002**, *418*, 964.
(6) Navarro, R. M.; Pena, M. A.; Fierro, J. L. G. *Chem. Rev.* **2007**, *107*, 3952.
(7) Ni, M.; Leung, M. K. H.; Leung, D. Y. C.; Sumathy, K. *Renewable Sustainable Energy Rev.* **2007**, *11*, 401.
(8) Hoffert, M. I.; Caldeira, K.; Jain, A. K.; Haites, E. F.; Harvey, L. D. D.; Potter, S. D.; Schlesinger, M. E.; Schneider, S. H.; Watts, R. G.; Wigley, T. M. L.; Wuebbles, D. J. *Nature* **1998**, *395*, 881.
(9) Fujishima, A.; Honda, K. *Nature* **1972**, *238*, 37.
(10) *Basic Research Needs for Solar Energy Utilization: Report on the Basic Energy Sciences Workshop in Solar Energy Utilization*; Argonne National Laboratory: Argonne, IL , 2005.
(11) Lehn, J. M.; Sauvage, J. P.; Ziessel, R. *Nouv. J. Chim.* **1980**, *4*, 623.
(12) Sato, S.; White, J. M. *Ind. Eng. Chem. Res.* **1980**, *19*, 542.
(13) Domen, K. N.; Shuichi; Soma, M.; Onishi, T.; Tamaru, K. *J. Chem. Soc., Chem. Commun.* **1980**, *12*, 543.
(14) Osterloh, F. E. *Chem. Mater.* **2007**, *20*, 35.
(15) Krol, R. v. d.; Liang, Y.; Schoonman, J. *J. Mater. Chem.* **2008**, *18*, 2311.
(16) Kudo, A. *Pure Appl. Chem.* **2007**, *79*, 1917.
(17) Maeda, K.; Domen, K. *J. Phys. Chem. C* **2007**, *111*, 7851.

Published on Web 04/02/2010

drawback of metal oxide systems is the typically large bandgaps (low visible absorption) or conduction bands too low in energy for hydrogen evolution.

In an attempt to address this shortcoming, significant research efforts have been directed to dye sensitization of metal oxide materials to improve visible light absorption and overall activity.[18−20] In addition, doping metal oxides with metal cations, carbon, sulfur, and nitrogen has been explored as a way to increase visible absorption.[21−25] Attempts have also been made to incorporate metal oxides into heterostructures to improve optical absorption and charge separation characteristics. Recent reports on the $BiVO_4$:Co_3O_4 system indicate enhanced photocatalytic activity and photoinduced charge separation when compared to the materials individually.[26,27] Studies on the ZrO_2:TiO_2 system also indicate that the interface between the two types of particle leads to diminished recombination.[28]

One promising class of materials for semiconductor photoelectrochemical purposes are the vanadates. In particular, a number of reports suggest that $InVO_4$ and $BiVO_4$ might be good candidate materials for photocatalysis.[16,29−34] However, the vanadates as a class are relatively unexplored especially when compared to well-known materials such as TiO_2 or ZnO. Given the success of these materials, we wondered whether incorporating $InVO_4$ into a heterostructure might provide synergies leading to enhanced activity. Given theoretical discussion about how cation exchange might affect the VO_4^{3-} band gap,[35] we also wondered whether using a cation like Tl might change the photoelectrochemical properties relative to In.

Utilizing this strategy, we report here the synthesis of $InVO_4$, $TlVO_4$, and an $InVO_4$:$TlVO_4$ composite by facile aqueous solution methods for the purpose of improving charge separation and the photoelectrochemical characteristics of the system. $InVO_4$ has two stable phases, monoclinic (*Cm*/2) and orthorhombic (*Cmcm*). Our work makes use of orthorhombic form of $InVO_4$.[36] Both $InVO_4$ and $TlVO_4$ share the orthorhombic *Cmcm* (63) crystal structure, which is composed of edge sharing (In/Tl)O_6 octahedra with VO_4 tetrahedral linkers. In and Tl have nearly identical atomic radii (1.93 Å and 1.96 Å, respectively[37]), which naturally leads to similar lattice dimensions and volumes for $InVO_4$[38] and $TlVO_4$[39] (325 $Å^3$ vs 345 $Å^3$, respectively). The similarity of crystal structure and dimension allows for $InVO_4$ to seed $TlVO_4$ growth, thereby providing an avenue for effective composite formation. These composites provide an opportunity to tune the band positions and study how these changes affect photoelectrochemical activity.

II. Experimental Section

Preparation of $InVO_4$. A 1 g portion (0.0085 mol) of NH_4VO_3 (Sigma-Aldrich, 99+% ACS Reagent grade) was dissolved in 125 mL of 60 °C water (Milli-Q UV Plus, 18.2 MΩ), and 3.342 g (0.0085 mol) of $In(NO_3)_3 \cdot xH_2O$ (Aldrich, 99.9% metals basis) was dissolved in 25 mL of water. After dissolution, the NH_4VO_3 solution was cooled to room temperature. $In(NO_3)_3 \cdot xH_2O$ solution was added to NH_4VO_3 solution resulting in a yellow/orange suspension. The suspension was heated to 100 °C and stirred under reflux conditions for 24 h. A yellow powder was isolated by vacuum filtration, washed with water (3 × 50 mL) and acetone (3 × 15 mL), and allowed to air-dry.

Preparation of $TlVO_4$. A 0.1319 g portion (0.001125 mol) of NH_4VO_3 was dissolved in 145 mL of 60 °C water, and 0.5 g of $Tl(NO_3)_3 \cdot 3H_2O$ (Aldrich, 98%) was dissolved in 5 mL of water with 5−10 drops of HNO_3 (Fisher, certified ACS Plus). After dissolution, the NH_4VO_3 solution was cooled to room temperature. $Tl(NO_3)_3 \cdot 3H_2O$ solution was added to NH_4VO_3 solution to immediately yield an orange suspension. The suspension was heated to 100 °C and stirred under reflux conditions for 24 h. An orange/brown powder was isolated by vacuum filtration, washed with water (3 × 50 mL) and acetone (3 × 15 mL), and allowed to air-dry.

Preparation of $InVO_4$:$TlVO_4$ Composite. A 0.1319 g portion of NH_4VO_3 was dissolved in 140 mL of 60 °C water, and 0.5 g $Tl(NO_3)_3 \cdot 3H_2O$ was dissolved in 5 mL of water with 5−10 drops of HNO_3. After dissolution, the NH_4VO_3 solution was cooled to room temperature, and 0.258 g (0.001125 mol) of $InVO_4$ was added to create a yellow suspension. To this suspension, the $Tl(NO_3)_3 \cdot 3H_2O$ was added dropwise (< 1 drop per second), creating a tan/brown suspension. The suspension was stirred at 100 °C under reflux conditions until a yellow suspension returned (1 h). This yellow powder was isolated by vacuum filtration, washed with water (3 × 50 mL) and acetone (3 × 15 mL), and allowed to air-dry.

Physical Characterization Methods. Powder X-ray diffraction (XRD) measurements were collected using a Rigaku D-MAX diffractometer using Cu Kα radiation operated at 45 kV and

(18) Kong, F. T.; Dai, S.-Y.; Wang, K.-J. *Adv. OptoElectron.* **2007**, *2007*, 1–13.
(19) Jose, R.; Thavasi, V.; Ramakrishna, S. *J. Am. Ceram. Soc.* **2009**, *92*, 289.
(20) Lenzmann, F. O.; Kroon, J. M. *Adv. OptoElectron.* **2007**, *2007*, 65073/1–65073/10.
(21) Kudo, A.; Niishiro, R.; Iwase, A.; Kato, H. *Chem. Phys.* **2007**, *339*, 104.
(22) Khan, S. U. M.; Al-Shahry, M.; Ingler, W. B., Jr. *Science* **2002**, *297*, 2243.
(23) Umebayashi, T.; Yamaki, T.; Yamamoto, S.; Miyashita, A.; Tanaka, S.; Sumita, T.; Asai, K. *J. Appl. Phys.* **2003**, *93*, 5156.
(24) Asahi, R.; Morikawa, T.; Ohwaki, T.; Aoki, K.; Taga, Y. *Science* **2001**, *293*, 269.
(25) Wu, G.; Nishikawa, T.; Ohtani, B.; Chen, A. *Chem. Mater.* **2007**, *19*, 4530.
(26) Long, M.; Cai, W.; Cai, J.; Zhou, B.; Chai, X.; Wu, Y. *J. Phys. Chem. B* **2006**, *110*, 20211.
(27) Long, C.; Kisch, H. *J. Phys. Chem. C* **2007**, *112*, 548.
(28) Siedl, N.; Elser, M. J.; Bernardi, J.; Diwald, O. *J. Phys. Chem. C* **2009**, *113*(36), 15792–15795.
(29) Zou, Z.; Ye, J.; Sayama, K.; Arakawa, H. *Nature* **2001**, *414*, 625.
(30) Ye, J.; Zou, Z.; Arakawa, H.; Oshikiri, M.; Shimoda, M.; Matsushita, A.; Shishido, T. *J. Photochem. Photobiol. A: Chem.* **2002**, *148*, 79.
(31) Ye, J.; Zou, Z.; Oshikiri, M.; Matsushita, A.; Shimoda, M.; Imai, M.; Shishido, T. *Chem. Phys. Lett.* **2002**, *356*, 221.
(32) Oshikiri, M.; Boero, M.; Ye, J.; Zou, Z.; Kido, G. *J. Chem. Phys.* **2002**, *117*, 7313.
(33) Dunkle, S. S.; Helmich, R. J.; Suslick, K. S. *J. Phys. Chem. C* **2009**, *113*, 11980.
(34) Kudo, A. *Int. J. Hydrogen Energy* **2006**, *31*, 197.
(35) Dolgos, M. R.; Paraskos, A. M.; Stoltzfus, M. W.; Yarnell, S. C.; Woodward, P. M. *J. Solid State Chem.* **2009**, *182*, 1964.
(36) Touboul, M.; Melghit, K.; Bénard, P.; Louër, D. J. Solid State Chem. 1995, *118*, 93–98.
(37) Lide, D. R., Atomic Radii of the Elements. *CRC Handbook of Chemistry and Physics*, 89th ed.; CRC Press/Taylor and Francis: Boca Raton, FL, 2009.
(38) Touboul, M.; Toledano, P. *Acta Crystallogr., Sect. B: Struct. Crystallogr. Cryst. Chem.* **1980**, *B36*, 240.
(39) Touboul, M.; Ingrain, D. *J. Less Common Met.* **1980**, *71*, 55.

20 mA, 1.5°/min scan rate, 0.02° step size. Samples were mounted on a glass slide using two-sided tape. Transmission electron microscopy (TEM) images were collected using a JEOL 2100 Cryo operating at 200 kV with samples supported on lacey Formvar/carbon 200 mesh copper grids (Ted Pella, Inc.). Energy Dispersive Spectroscopy (EDS) spectra were collected using a JEOL 2010F STEM equipped with an EDS probe. Diffuse reflectance UV−visible measurements were taken using a Varian Cary 5G spectrophotometer and transformed into absorbance units by the Kubelka−Munk relationship $K/S = (1 - R)^2/(2R)$ where R is reflectance, K is the absorption coefficient, and S is twice the scattering coefficient.[40]

Photoelectrochemical Measurements. Working electrodes were constructed by depositing sample onto indium tin oxide coated glass slides (70−100 Ω/sq surface resistivity, Aldrich) previously rinsed with isopropanol. Sample slurry in ethanol was dropped onto an area marked off by scotch tape. After being air-dried with the tape removed, electrodes were heated at 200 °C for 12 h. Copper wire was brought into contact with ITO using InGa eutectic (99.99+%, Aldrich) and adhered using epoxy. Electrochemical measurements were performed using a CHI 760C bipotentiostat (CH Instruments) with a platinum gauze counter electrode and a Ag/AgCl reference electrode. All potentials are reported in reference to Ag/AgCl. A xenon arc lamp (Newport) operated at 150 W and equipped with a water filter was used to irradiate samples from the back side of the electrode, which reduces the influence of semiconductor film thickness.[27] The photoelectrochemical cell has a circular sample port of 1 cm diameter, which allows for an electrode area of 0.785 cm^2. A 0.1 M K_2SO_4 (99.99% metals basis, Aldrich) solution, adjusted to pH = 4 by H_2SO_4,was used as the electrolyte. Electrolyte was purged for 20 min with Ar before measurements, and a positive Ar pressure over the solution was maintained during experiments. The apparatus was fitted with a 400 nm cutoff filter (Edmund Industrial Optics) to test visible light response.

Band Structure Determination. Density Functional Theory (DFT)[41] calculations were performed using the CASTEP[42] code within Materials Studio 4.4 (Accelrys).[43] Three dimensional periodic cells were constructed from the published space group and crystal structure parameters of $InVO_4$[38] and $TlVO_4$.[39] Atomic coordinates were approximated for $TlVO_4$ because of lack of published data; the structure was geometrically optimized before proceeding. The band structure of the composite was obtained by layering the cell of $InVO_4$ with that of $TlVO_4$ to form a new supercell containing the unit cell of both materials. Calculations were performed within the generalized gradient approximation (GGA)[44,45] using the Perdew−Burke−Ernzerhof (PBE)[46] exchange-correlation functional. Band structure and partial density of state determinations were carried out with ultrasoft pseudopotentials, $4 \times 4 \times 3$ k-point density, 5.0×10^{-7} eV/atom SCF tolerance, density mixing electronic minimization, fixed orbital occupancy, 380 eV energy cutoff, and density of states integration by the interpolation method.

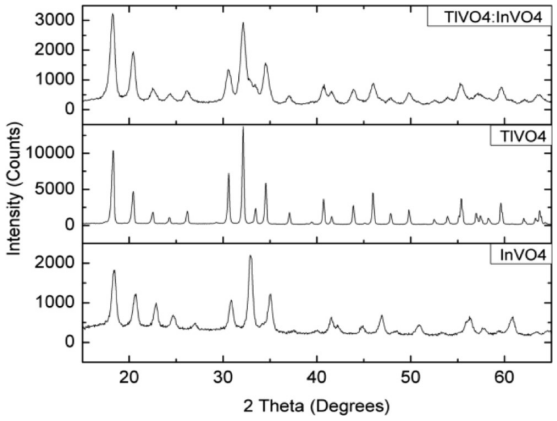

Figure 1. X-ray diffractograms of $InVO_4$:$TlVO_4$ composite, $TlVO_4$, and $InVO_4$.

III. Results and Discussion

$InVO_4$ is typically synthesized by a solid state method involving the reaction of In_2O_3 and V_2O_5 at high temperature.[31,47] Sample particles made by this method tend to be large and have a correspondingly low surface area. Also reported are wet chemical precipitation methods followed by subsequent calcination at around 600 °C.[48,49] The synthetic method reported here differs from previous approaches to making $InVO_4$. The reflux conditions of the aqueous environment at pH = 4 induce crystallization of nanoparticulate orthorhombic $InVO_4$ that is ordinarily accessed at temperatures above 680 °C.[48] These same conditions also lead to crystallization of orthorhombic $TlVO_4$.

Figure 1 shows powder X-ray diffraction data of $InVO_4$, $TlVO_4$, and $InVO_4$:$TlVO_4$ composite. The $InVO_4$ diffractogram features broad, low intensity peaks indexed to orthorhombic $InVO_4$ (JCPDS no. 04−008−7237).[38] The peak broadening apparent in the diffractogram arises as a consequence of the small $InVO_4$ crystallite size (vide infra).

The $TlVO_4$ diffractogram contains sharp, intense peaks which match orthorhombic $TlVO_4$ (JCPDS no. 35−0086)[39] well. Minor deviations in diffractogram intensities in the low angle region between that reported here and that reported by Touboul and Ingrain[39] are likely caused by different preferred orientations or preparation methods between the crystals studied.[50] The diffractogram for the $InVO_4$:$TlVO_4$ composite matches that of $TlVO_4$, but with contributions from $InVO_4$ apparent as shoulders or broadened peaks; $InVO_4$ peaks appear roughly 0.5° higher in 2θ than $TlVO_4$ peaks. This observation indicates that both $InVO_4$ and $TlVO_4$ were synthesized and are present in the composite sample.

Figure 2 shows TEM micrographs of $InVO_4$, $TlVO_4$, and the $InVO_4$:$TlVO_4$ composite. Images A and B contain

(40) Mirabella, F. M. *Modern Techniques in Applied Molecular Spectroscopy*; John Wiley & Sons: New York, 1998.
(41) Kohn, W.; Sham, L. J. *Phys. Rev. A* **1965**, *140*, 1133.
(42) Clark, S. J. S.; Matthew, D.; Pickard, C. J.; Hasnip, P. J.; Probert, M. I. J.; Refson, K.; Payne, M. C. *Z. Kristallogr.* **2005**, *220*(5−6), 567.
(43) Accelrys; Software; Inc. *Materials Studio Release Notes*, Release 4.4; Accelrys Software Inc.: San Diego, CA, 2008.
(44) Perdew, J. P.; Wang, Y. *Phys. Rev. B* **1992**, *45*, 13244.
(45) Perdew, J. P.; Chevary, J. A.; Vosko, S. H.; Jackson, K. A.; Pederson, M. R.; Singh, D. J.; Fiolhais, C. *Phys. Rev. B* **1992**, *46*, 6671.
(46) Perdew, J. P. B., K.; Ernzerhof, M. *Phys. Rev. Lett.* **1996**, *77*, 3865.
(47) Lin, H.-Y.; Chen, Y.-F. *Int. J. Hydrogen Energy* **2007**, *32*, 86–92.
(48) Denis, S.; Baudrin, E.; Touboul, M.; Tarascon, J. M. *J. Electrochem. Soc.* **1997**, *144*, 4099–4109.
(49) Baudrin, D.; Orsini; Seguin; Touboul; Tarascon *J. Mater. Chem.* **1999**, *9*, 101–105.
(50) Bish, D. L.; Reynolds, R. C. *Rev. Mineral. Geochem.* **1989**, *20*, 73.

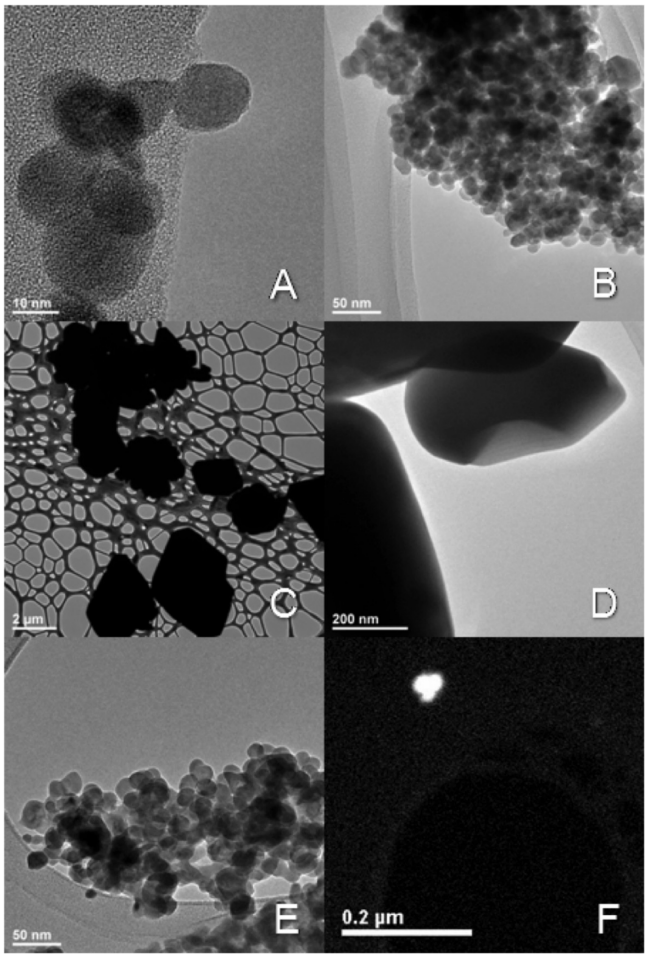

Figure 2. TEM images of (A, B) $InVO_4$, (C, D) $TlVO_4$, and (E) $InVO_4$:$TlVO_4$ composite, and (F) a STEM image of the $InVO_4$:$TlVO_4$ composite.

$InVO_4$ nanoparticles ranging from 10 to 30 nm in diameter and agglomerated into large clusters of discernible particles. The small size of these particles is consistent with the diffractogram peak broadening discussed above. Images C and D display $TlVO_4$ particles which range from 1 to 5 μm in diameter. $TlVO_4$ particles do not agglomerate and appear smooth with few surface defects. $TlVO_4$ generally melts under focused, high energy e^- beam while $InVO_4$ particles are robust and able to dissipate the injected charge. Previous studies have indicated that $TlVO_4$ is susceptible to decomposition above 300 °C,[39,51] which explains the e^- beam sensitivity of this system.

Image E contains a TEM image of $InVO_4$:$TlVO_4$ composite nanoparticles between 20 and 40 nm in diameter with significant agglomeration into clusters. These clusters are altered in shape by the e^- beam, though not as strongly as is $TlVO_4$, which causes individual particles to fuse into larger masses. Image F displays a small cluster of composite material collected by scanning TEM (STEM). The particles in images E and F show no evidence of a core−shell boundary or any other type of distinct heterostructure visible by TEM.

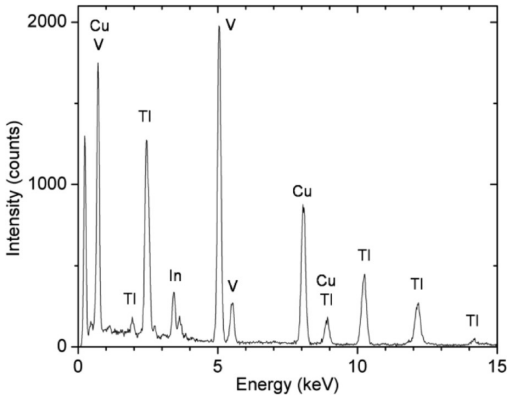

Figure 3. EDS spectrum of $InVO_4$:$TlVO_4$ composite.

Figure 3 displays the EDS spectrum of $InVO_4$:$TlVO_4$ composite taken in STEM mode. The EDS spectrum of the composite was collected to determine whether $TlVO_4$ was successfully deposited onto the surface of $InVO_4$ nanoparticles. EDS indicates the presence of Tl, In, and V in the $InVO_4$:$TlVO_4$ composite sample. Measurements performed on agglomerated regions as well as individual particles and small clusters revealed comparable ratios of indium and thallium throughout the sample, which excludes the possibility of separate domains of $TlVO_4$ and $InVO_4$. The presence of oxygen prevents accurate quantitative analysis of sample composition because of selective low energy X-ray absorbance by the beryllium window of the EDS detector.[52] Extraneous peaks of copper originate from the supporting grid. Thus, XRD confirms the presence of orthorhombic $InVO_4$ and $TlVO_4$, indicating that both crystal systems have been incorporated into the composite material. The lack of definable structure between the two materials in TEM images is likely the result of nearly identical crystal structures, allowing growth of $TlVO_4$ to take place on the $InVO_4$ crystals without significant strain being introduced.

Figure 4 shows cyclic voltammograms of $InVO_4$, $TlVO_4$, and $InVO_4$:$TlVO_4$ composite under no illumination, full xenon arc lamp illumination, and xenon arc lamp illumination with a 400 nm cutoff filter. Photocurrent density measurements were compiled at −0.5 V, 0 V, and 1 V in table 1. Samples show anodic photocurrent with onset of 0.25 V for $InVO_4$ and roughly 0.35 V for both $TlVO_4$ and the composite material. $TlVO_4$ shows roughly a 10-fold increase in anodic photocurrent over $InVO_4$ while the composite shows a 2-fold increase. Illumination also increases cathodic photocurrent in each sample, with significant photocurrent increases and potential onsets of 0.3 V for $InVO_4$ and 0.4 V for $TlVO_4$ and the composite. Again, both the $TlVO_4$ and the composite show more than a 10-fold increase in cathodic photocurrent over $InVO_4$.

There exist several possible explanations for the larger photocurrent density exhibited by $TlVO_4$ and $InVO_4$:$TlVO_4$ composite. Ordinarily, one would expect a sample with larger electrochemical surface area (smaller particles) to display more photoelectrochemical activity; however,

(51) Touboul, M.; Cuche, C.; Ganne, M.; Tournoux, M. *Z. Anorg. Allg. Chem.* **1974**, *410*, 1.

(52) Goodhew, P. J., Humphreys, J., Beanland, R. *Electron Microscopy and Analysis*, 3rd ed.; Taylor and Francis: New York, 2001.

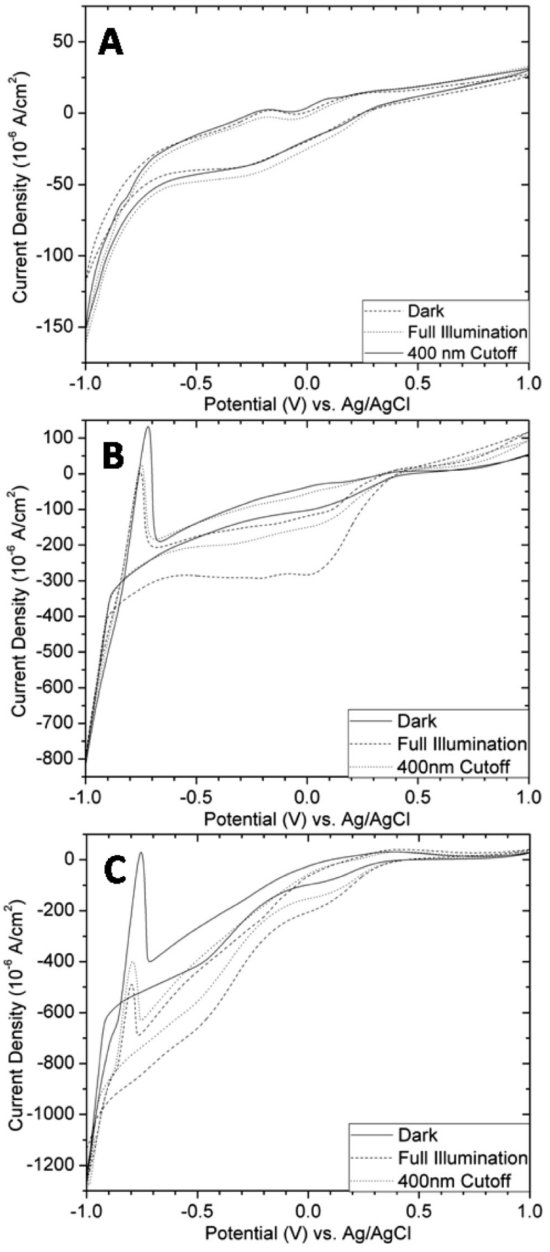

Figure 4. Cyclic voltammetry of (A) $InVO_4$, (B) $TlVO_4$, (C) $InVO_4$:$TlVO_4$ composite performed at pH = 4 in 0.1 M $K_2SO_{4(aq)}$.

the response of our samples is counter to the results that may be expected based on particle size considerations alone. The $TlVO_4$ particles are at least an order of magnitude larger than $InVO_4$ and should correspondingly have a smaller surface area and thus lower electrochemical activity, but $TlVO_4$ exhibits a greater photoelectrochemical response. Disparate film thicknesses could also account for different photoelectrochemical; however, we controlled the film thickness of all samples studied to 10 μm. These observations strongly suggest that the differences in photoelectrochemical activity relate to differences in materials chemistry.

Typically, for an n-type semiconductor, no cathodic photocurrent is observed as photocurrent is the result of minority carrier generation and subsequent oxidation of solution species. However, previous research has noted

Table 1. Photocurrent at 1 V, 0 V, and −0.5 V

	Photocurrent Density (μA/cm^2)		
	$InVO_4$	$TlVO_4$	$InVO_4$:$TlVO_4$
1 V	5.56	63.30	11.91
0 V	−5.37	−180.38	−108.31
−0.5 V	−8.19	−105.86	−245.61

the occurrence of an anomalous photoeffect (APE) in semiconductors arising from surface states within the energy bandgap, which could be the origin of anomalous cathodic photocurrent in $InVO_4$, $TlVO_4$, and the composite.[53,54] In each sample, the I−V curve has a general tilt indicative of redox processes on the surface, particularly as vanadium oxoanions are progressively oxidized or reduced.

Figure 4 shows that both the $TlVO_4$ and $InVO_4$:$TlVO_4$ composite contain a reversible redox couple near −0.8 V which is attributable to the Tl^0/Tl^+ couple ($E_0 = -0.336$ V + 0.0591 log[Tl^+] V). Studies on $TlVO_3$, which contains Tl^+, also indicate the same type of reversible redox peaks. Tl^{3+} is reduced to Tl^+ according to the Tl^+/Tl^{3+} redox couple at $E_0 = 1.252$ V, resulting in Tl^+ at the surface that is reduced to Tl.[55] However, the photoactivity of $TlVO_4$ and $InVO_4$:$TlVO_4$ composite is the same if the potential is reversed prior to accessing the Tl^+/Tl^0 couple.

Figure 5 shows Mott−Schottky plots constructed from capacitance measurements collected by alternating current (AC) voltammetry. This data was transformed to $1/C^2$ to fit the Mott−Schottky equation

$$\frac{1}{C_{SC}^2} = \left[\frac{2}{e\varepsilon\varepsilon_0 N_D}\right]\left[E - E_{fb} - \frac{kT}{e}\right]$$

where C_{sc} is the space charge capacitance, e is the electron charge, k is the Boltzmann constant, T is temperature in Kelvin, ε_0 is the permittivity of free space, ε is the dielectric constant of the film electrode, N_D is the carrier density, and E and E_{fb} are the applied and flatband potentials, respectively.[56,57] When plotted, $1/C^2$ versus E is linear in the depletion region of the semiconductor and allows estimation of flat-band potential, E_{fb}, at the intersection of the potential axis ($1/C^2 = 0$).[58] The flat-band potential provides a good estimation of the conduction band edge in n-type semiconductors.[59] The band edge generally lies between 0.1 and 0.4 eV more negative depending upon conductivity of the semiconductor.[60] As compiled in Table 2, estimated flat band potentials are

(53) Müller, N.; Hodes, G.; Vainas, B. *J. Electroanal. Chem.* **1984**, *172*, 155.
(54) Morisaki, H.; Hariya, M.; Yazawa, K. *Appl. Phys. Lett.* **1977**, *30*, 7.
(55) Pourbaix, M. *Atlas of Electrochemical Equilibria in Aqueous Solutions*, 2nd ed.; National Association of Corrosion Engineers: Houston, TX, 1974.
(56) Cho, I.-S.; Lee, S.; Noh, J. H.; Choi, G. K.; Jung, H. S.; Kim, D. W.; Hong, K. S. *J. Phys. Chem. C* **2008**, *112*, 18393.
(57) Khan, S. U. M.; Akikusa, J. *J. Phys. Chem. B* **1999**, *103*, 7184.
(58) Bard, A. J., Faulkner, L. R. *Electrochemical Methods: Fundamentals and Applications*, 2nd ed.; John Wiley & Sons, Inc.: Singapore, 2004.
(59) Hashiguchi, H.; Maeda, K.; Abe, R.; Ishikawa, A.; Kubota, J.; Domen, K. *Bull. Chem. Soc. Jpn.* **2009**, *82*, 401.
(60) Matsumoto, Y. *J. Solid State Chem.* **1996**, *126*, 227.

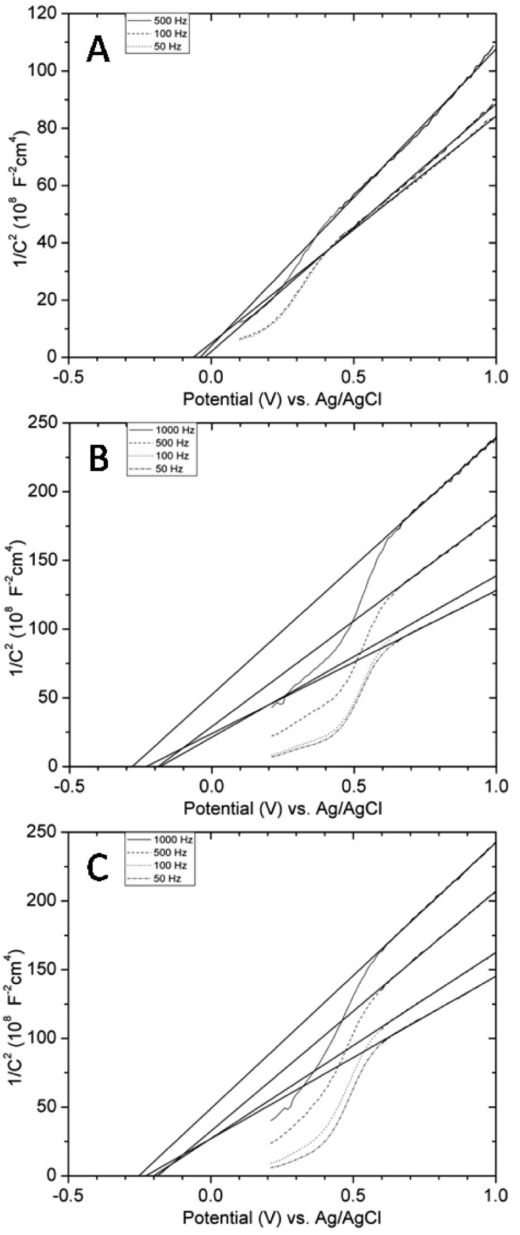

Figure 5. Mott−Schottky plots of (A) $InVO_4$, (B) $TlVO_4$, and (C) $InVO_4$:$TlVO_4$ composite performed in pH = 4 0.1 M $K_2SO_{4(aq)}$.

−0.041 V, −0.221 V, and −0.217 V versus Ag/AgCl for $InVO_4$, $TlVO_4$, and the $InVO_4$:$TlVO_4$ composite, respectively. These flat-band potentials give some insight into the photoactivity of the materials with water. Samples containing Tl appear to have a conduction band edge more negative than that of $InVO_4$, possibly allowing for better water reduction activity. None of the materials studied, however, has band positions ideal for photocatalytic water splitting without application of an electrochemical bias ($E°[H^+/H_2]$ = −0.236 V vs NHE at pH = 4, −0.458 V vs Ag/AgCl).[61]

We recognize that our estimation of the conduction band level is at odds with reported observation of H_2 production from $InVO_4$ and $InVO_4$ loaded with Ni/NiO. Our own experience suggests that little or no H_2 is produced from samples of $InVO_4$. Additionally, there exist several potential experimental complications that could render a higher level of uncertainty into the results. Even in the case where the conduction band level of $InVO_4$ is around 0.4 eV more negative than the flatband potential, there will be little or no overpotential to perform the water reduction reaction, which leads to minimal H_2 production from H_2O.

Table 2. Flat-Band Potentials Determined from Mott−Schottky Method

	flat band potential (V) vs Ag/AgCl		
frequency	$InVO_4$	$TlVO_4$	$InVO_4$:$TlVO_4$ composite
1000 Hz	N/A	−0.280	−0.253
500 Hz	−0.038	−0.189	−0.186
100 Hz	−0.023	−0.182	−0.200
50 Hz	−0.063	−0.231	−0.228
average	**-0.041**	**-0.221**	**-0.217**

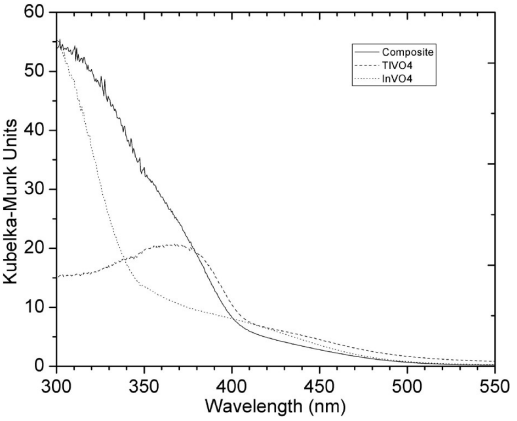

Figure 6. UV−visible diffuse reflectance spectra of $TlVO_4$, $InVO_4$, and $InVO_4$:$TlVO_4$ composite.

Figure 6 contains diffuse reflectance UV−vis spectra of $TlVO_4$, $InVO_4$, and $InVO_4$:$TlVO_4$ composite samples. Band gaps for samples are estimated by extrapolation of the linear portion of the absorption edge. Bandgaps for $InVO_4$, $TlVO_4$, and $InVO_4$:$TlVO_4$ are estimated as 3.50 eV (354 nm), 2.98 eV (422 nm), and 2.94 eV (415 nm), respectively. The presence of thallium in $TlVO_4$ and the composite serves to reduce the bandgap of these vanadates relative to $InVO_4$.

Figure 6 also reveals the presence of absorption in the visible wavelengths for each sample extending to approximately 600 nm (2.07 eV) for $InVO_4$ and the composite and roughly 800 nm (1.55 eV) for $TlVO_4$. Previous reports of the band gap of $InVO_4$ by diffuse reflectance UV−visible spectroscopy have typically estimated it as 1.9−2.0 eV.[30,31,62,63] The $InVO_4$ bandgap presented here significantly deviates from those of previous reports. Interestingly, we performed photoluminescence measurements on the $InVO_4$ material (not

(61) Lide, D. R., Electrochemical Series. *CRC Handbook of Chemistry and Physics*, 89th ed.; CRC Press, Taylor and Francis: Boca Raton, FL, 2009.

(62) Zhang, L.; Fu, H.; Zhang, C.; Zhu, Y. *J. Solid State Chem.* **2006**, *179*, 804.

(63) Yao, J.-M.; Lee, C.-K.; Yang, S.-J.; Hwang, C.-S. *J. Alloys Compd.* **2009**, *481*, 740.

Table 3. Comparison of Calculated and Experimental Band Gaps

	calculated band gap (eV)	experimental band gap (eV)
$InVO_4$	3.14	3.50
$TlVO_4$	1.92	2.94
$InVO_4$:$TlVO_4$ composite	2.25	2.98

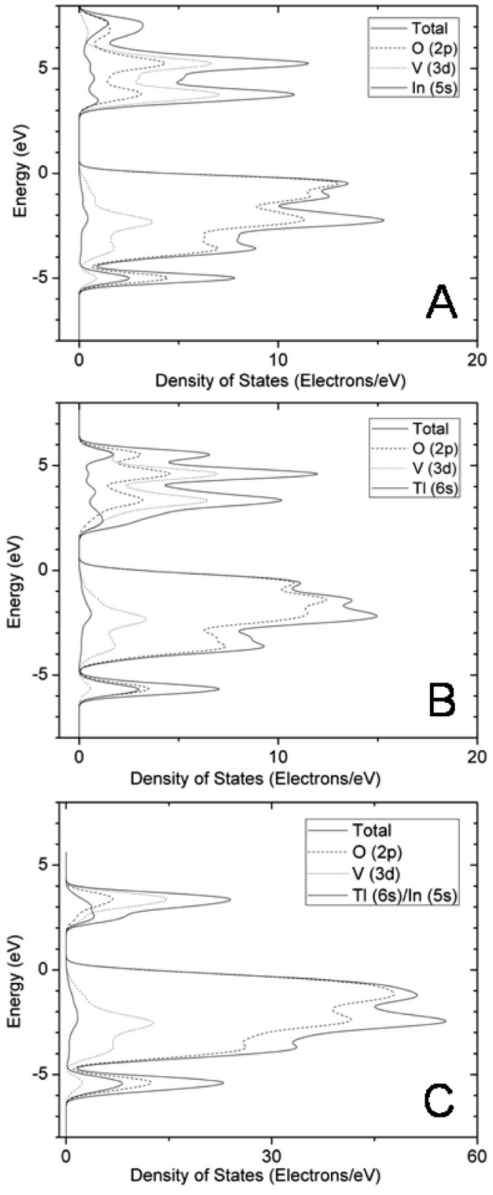

Figure 7. Partial density of states (PDOS) of (A) $InVO_4$, (B) $TlVO_4$, and (C) $InVO_4$:$TlVO_4$ composite. (PDOS labeled by primary contribution to s, p, and d orbitals).

shown). These measurements revealed the presence of a luminescence peak at 550 nm with 325 nm excitation, but no luminescence was observed with 442 nm excitation. These results suggest that the $InVO_4$ band gap is at energies greater than 442 nm (or 2.8 eV).

To better understand these observations, DFT calculations were performed to elucidate the band structure. Figure 7 presents the partial density of states of the materials as calculated using the CASTEP code within Materials Studio 4.4. The 0 eV energy signifies the highest occupied state of the semiconductor, corresponding to the top of the valence band. The calculated bandgap of $InVO_4$, $TlVO_4$, and the $InVO_4$:$TlVO_4$ composite is 3.14 eV, 1.92 eV, and 2.25 eV, respectively as shown in Table 3. The bandgap for $InVO_4$ correlates well with the 3.1 eV predicted by Oshikiri et al. in previous studies,[32,64] though is larger than the 2.3 eV calculated by Zhang and co-workers.[62] Results from these calculations match well with UV−vis observations and are consistent with bandgap underestimation typical of DFT calculations.[35,65−67]

The origin of the visible absorbance for $InVO_4$, $TlVO_4$, and the composite likely arise from oxygen vacancies and gap states lying above the valence band. These states lie closer to the conduction band and give rise to false band edges, albeit with significant absorption, that are lower in energy than the true bandgap. Similar observations are seen with $InTaO_4$, for which it has been determined that the apparent optical bandgap of 2.6 eV[68] actually arises from oxygen vacancy levels within the bandgap[67,69] while the true optical bandgap is 4.3 eV.[67] A valence band to conduction band transition of 3.50 eV for $InVO_4$, as measured by diffuse reflectance UV−vis spectroscopy, is not surprising as calculations have predicted $InVO_4$ to have a smaller bandgap relative to $InTaO_4$ (3.1 eV vs 3.7 eV) because V 3d orbitals lie at lower energy, likely because of higher electronegativity and different crystal geometry.[32] $TlVO_4$, however, has lower energy band edge absorption at 2.94 eV with significant deviation from the predicted 1.92 eV bandgap. One reason this underestimation is so large could be the presence of a conduction band with more s orbital character, which has previously been shown to give rise to band gap determination errors exceeding 2 eV in DFT calculations.[70−72] While the inaccuracies associated with uncorrected DFT bandgap calculations may be large, the DFT calculations still provide a point of comparison. The systems we study are similar enough in nature that the inaccuracies resulting from discontinuity in the exchange correlation functional and other correlation effects should be similar and allow evaluation of relative band positions and composition.

Our DFT calculations indicate that the primary contribution to the valence band of each compound comes from O 2p orbitals with small contributions from V 3d, In 5s, and/or Tl 6s and 6p. The valence bands of both $InVO_4$ and $TlVO_4$ would ordinarily be expected to occur at nearly the same level because of the dominant contribution of O 2p orbitals and the small energy difference between In and Tl. Estimation of the valence bands by the Mott−

(64) Oshikiri, M.; Boero, M.; Ye, J.; Aryasetiawan, F.; Kido, G. *Thin Solid Films* **2003**, *445*, 168.
(65) Perdew, J. P.; Levy, M. *Phys. Rev. Lett.* **1983**, *51*, 1884.
(66) Zunger, A.; Perdew, J. P.; Oliver, G. L. *Solid State Commun.* **1980**, *34*, 933.
(67) Matsushima, S.; Obata, K.; Nakamura, H.; Arai, M.; Kobayashi, K. *J. Phys. Chem. Solids* **2003**, *64*, 2417.
(68) Zou, Z.; Ye, J.; Arakawa, H. *Chem. Phys. Lett.* **2000**, *332*, 271.
(69) Chang, H.; Kong, K.; Choi, Y. S.; In, E.; Choi, Y.; Baeg, J.-O.; Moon, S.-J. *Chem. Phys. Lett.* **2004**, *398*, 449.
(70) Walsh, A.; Yan, Y.; Huda, M. N.; Al-Jassim, M. M.; Wei, S.-H. *Chem. Mater.* **2009**, *21*, 547.
(71) Janotti, A.; Van de Walle, C. G. *Phys. Rev. B* **2007**, *76*, 165202.
(72) Lany, S.; Zunger, A. *Phys. Rev. B* **2008**, *78*, 235104.

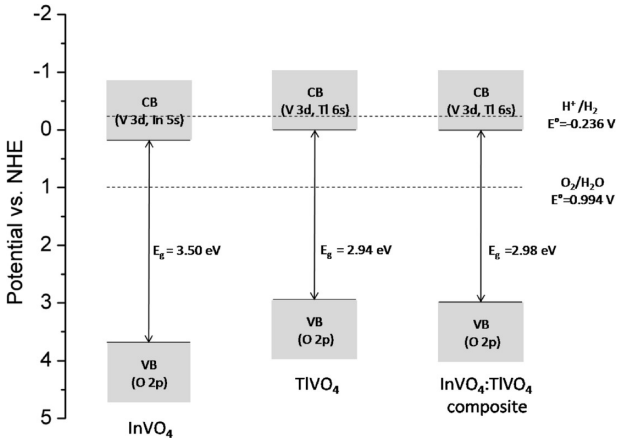

Figure 8. Representation of the band structures of $InVO_4$, $TlVO_4$, and $InVO_4$:$TlVO_4$ composite at pH 4.

Schottky method coupled with UV−visible measurements, however, indicates the valence band tops of $TlVO_4$ and the composite lies nearly 0.7 eV more negative than that of $InVO_4$. A schematic representation of the proposed band structures of these compounds based upon Mott−Schottky flat-band potentials and UV−visible bandgap approximations is presented in Figure 8. Calculations performed by Walsh et al. on $BiVO_4$ show that Bi 6s interaction with O 2p causes an upward dispersion in the maximum energy of the valence band of 0.4 eV.[70] The presence of Tl 6s and 6p orbitals and their coupling with O 2p orbitals in $TlVO_4$ and the composite thus could be the cause of the higher valence band edges. Coupling between Tl 6s and O 2p in the valence band is qualitatively apparent as delocalization of the density of states when compared to that of $InVO_4$ where sharper, more localized states exist.

The conduction bands of both $TlVO_4$ and $InVO_4$ are primarily composed of V 3d orbitals with additional contribution from O 2p, In 5s, and/or Tl 6s, matching previous observations.[62] The contribution of Tl 6s orbitals, in contrast to In 5s orbitals, provides a more hybridized conduction band in $TlVO_4$ which again appears to slightly raise the conduction band bottom relative to that of $InVO_4$.

The diffuse nature of the Tl 6s orbitals incorporated into the conduction band and valence band of $TlVO_4$ allows better contact and interaction with solution species. The Gerischer model of semiconductor-electrolyte interfaces suggests that the rate of reaction is dependent upon the overlap of the density of states of the semiconductor valence band and conduction band with the reactants.[58,73] The more diffuse s orbitals incorporated into the conduction band of $TlVO_4$ would thus exhibit improved contact with the electrolyte and could result in greater photocurrent. Indeed, this is what is seen in Figure 4 for the Tl-containing species; s orbitals are available at the bottom of the conduction band to accept photogenerated electrons to reduce water when sufficiently negative potentials are reached. This effect is most likely enhanced by increased absorption into the visible region of the spectrum because of the lower energy bandgap of the $TlVO_4$. An alternative explanation for the different photocurrent densities of the materials could be differences in the photoelectrochemical surface area available because of different particle size and shape. The evidence contradicts this assumption, however, because more photocurrent occurs for lower surface area $TlVO_4$ than either $InVO_4$ or $InVO_4$:$TlVO_4$ composite as discussed above.

The $InVO_4$:$TlVO_4$ composite material is dominated by $TlVO_4$ characteristics despite the fact that both $InVO_4$ and $TlVO_4$ are incorporated into the composite as inferred by XRD, TEM, and EDS. UV−vis shows the composite shares similar band edge absorptions with $TlVO_4$ with some small contribution from $InVO_4$. Photoelectrochemistry shows nearly identical flat band potentials and similar photoactivity; this result is not surprising since the synthetic method utilized deposits $TlVO_4$ onto the surface of $InVO_4$, thereby yielding surfaces of similar chemistry for $TlVO_4$ and the composite. The calculations also reinforce the dominant effect of Tl in the composite by yielding a similar band structure and density of states to that of $TlVO_4$.

IV. Conclusion

In summary, we report a simple solution method to synthesize $InVO_4$, $TlVO_4$, and an $InVO_4$:$TlVO_4$ composite. Photoelectrochemical activity and the band structure of $TlVO_4$ has been characterized for the first time and compared to the better characterized $InVO_4$. We conclude from these results that the higher photoelectrochemical activity of $TlVO_4$ and the $InVO_4$:$TlVO_4$ composite arise from the more diffuse Tl 6s character of the valence and conduction bands relative to In; this enables better contact with electrolyte allowing photogenerated electrons and holes to more readily react with solution species, which decreases the likelihood of charge recombination. The results reported here provide the first evaluation of $TlVO_4$ as a photocatalyst and evidence that incorporating crystallographically similar metal oxides into a composite heterojunction can alter the band positions and bandgap, providing an opportunity for concerted band engineering and tuning. Figure 8 graphically presents this band tuning and gives better approximations of the valence and conduction band positions than those previously published.

Acknowledgment. TEM, STEM, XRD, and diffuse reflectance UV−visible spectroscopy were carried out in part in the Frederick Seitz Materials Research Laboratory Central Facilities, University of Illinois, which are partially supported by the U.S. Department of Energy under Grants DE-FG02-07ER46453 and DE-FG02-07ER46471. This work was supported by the National Science Foundation.

Supporting Information Available: Figure SI 1 of the photoluminescence of $InVO_4$. This material is available free of charge via the Internet at http://pubs.acs.org.

(73) Licht, S. *Encyclopedia of Electrochemistry: Semiconductor Electrodes and Photoelectrochemistry*; Wiley-VCH: Weinheim, Germany, 2002; Vol. *6*.